REVISTA MATÉRIA V.28 N.3
ISSN 1517-7076 articles e20230147, 2023

Investigation of specimen size effect on the use of double punch test as quality control method of the steel fiber reinforced shotcrete

Felipe Pereira Santos[1], Alan Renato Estrada Cáceres[1], Rafael Celeghini Santiago[2,3], Antonio Domingues de Figueiredo[1], Luís Antônio Guimarães Bitencourt Júnior[4]

[1]Universidade de São Paulo, Escola Politécnica, Departamento de Engenharia de Construção Civil. Avenida Professor Almeida Prado, Trav. do Biênio, 83, 05508-070, São Paulo, SP, Brasil.

[2]Universidade Federal do ABC, Centro de Engenharia, Modelagem e Ciências Sociais Aplicada. Alameda da Universidade, 3, Anchieta, 09606-070, São Bernardo do Campo. SP, Brasil.

[3]Technology Innovation Institute, Advanced Materials Research Centre. Abu Dhabi, United Arab Emirates.

[4]Universidade de São Paulo, Escola Politécnica, Departamento de Engenharia de Estruturas e Geotécnica. Avenida Professor Almeida Prado, Trav. do Biênio, 83, 05508-070, São Paulo, SP, Brasil.

e-mail: felipe.pereira.santos@usp.br, alan.estrada@usp.br, rafael.santiago@ufabc.edu.br, antonio.figueiredo@usp.br, luis.bitencourt@usp.br

ABSTRACT

The double punch test (DPT) is increasingly used internationally for quality control of steel fiber reinforced shotcrete (SFRS). This study intends to verify the influence of the DPT specimens' diameter on the residual strength behavior of the SFRS. The experimental program aims to evaluate the dynamics of the test in terms of the results obtained from the analytical conversion of the axial displacement into total circumferential opening displacement (TCOD). The results are compared to those obtained through the 3D digital image correlation (DIC3D) to evaluate its applicability as a quality control method of the SFRS. The results demonstrated that the TCOD could be easily obtained by analytical conversion with reliable accuracy. The analysis of the DPT results could consider the crack opening level to obtain constitutive equations. The diameter of the DPT specimens directly influences the structural parameters of the SFRS. Smaller specimens may show a 35% reduction in residual strength associated with the service limit state. As the coefficient of variation of the residual strength associated with the ultimate limit state practically doubles when smaller specimens are used, for the same reliability, the sample sizing of the specimens of 10 cm is twice the quantity of the 15 cm.

Keywords: Steel fiber reinforced shotcrete; Tunneling quality control; Double punch test; Inductive test; Digital image correlation.

1. INTRODUCTION

Over the years, fiber reinforced shotcrete (FRS) has widely spread in infrastructure construction. FRS is particularly interesting for slope contention works and tunnel linings in geotechnical applications. This last application is strongly linked to the NATM (New Austrian Tunneling Method). It aims to mobilize the soil strength capacity to ensure lower stress levels in the structural lining since loads are redistributed without loss of structural competence [1].

During the application of the FRS, most of the shotcrete volume remains at the surface, but part of the constituent materials is non-uniformly rebounded [2]. The rebound intensity varies depending on several factors, such as spraying velocity and impacting surface [3, 4]. One of the constituents that may have its composition most affected by the rebound phenomenon is steel fiber [5, 6]. These facts may result in a divergence between the designed fiber content from that incorporated and the mechanical properties of FRS. These divergences lead to uncertainties regarding the structural behavior of the FRS.

The post-crack strength capacity is correlated with the fiber-matrix interaction of the FRS, which justifies that quality control of the composite is historically carried out by assessing the toughness-related properties [7] and the fresh state [8]. In this context, the most common tests in FRS guidelines to perform the residual strength capacity quality control are the square panel test (EN14488-5 [9]) and the bending beam test (EN14488-3 [10]). Using these test methods allows classified FRS according to the energy absorbed by the specimen performing

Corresponding Author: Antonio Figueiredo Received on 10/05/2023 Accepted on 21/08/2023

DOI: https://doi.org/10.1590/1517-7076-RMAT-2023-0147

the square panel test or considering the post-crack strengths measured with the flexural beam test. Both procedures are unfeasible for extracting the specimen directly from the structure [3, 11]. In that sense, the double punch test (DPT) can be easily performed using cores extracted from the tunnel lining.

The steel fiber content incorporated is typically assessed by washing the FRS and counting or weighing the fibers (EN14488-7 [12]). However, there are non-destructive alternatives for smaller specimens, such as the inductive test, which is preferable for being a faster and more robust method [13–15]. In addition, this methodology is feasible to assess the orientation of the fibers in the specimen, which is a relevant input in numerical models for residual capacity behavior prediction [15–20]. Consequently, a single core extracted from the tunnel lining can provide relevant information on fiber content and assess the mechanical behavior.

Nowadays, there is a growing concern to improve the monitoring and evaluation [21, 22] of the structural condition of infrastructure projects. In this sense, special techniques such as acoustic emission [23] and piezoelectric transducers [24] can be very useful for checking the health conditions of the structure. However, there will still be difficulties in connecting this information with the typical requirements used for the specification and design of tunnel linings, such as energy absorption [25] and material parameterization to obtain constitutive models [11]. The double punch test could be a suitable complement to the evaluation of structures integrating these two approaches [26] together with other monitoring techniques.

A significant concern is related to the safety of test operators in laboratories. In this context, the DPT is also an attractive alternative test once the specimens are smaller, 15 cm or 10 cm in height and diameter, and easier to handle concerning the traditional tests. Therefore, there is a reduction in the risk of injuries during its manipulation, and it is possible to increase the frequency of tests with lower volumes of shotcrete. Considering these advantages, some studies endorse the DPT as a feasible alternative for FRS control [3, 27]. In addition, this test method correlates well with energy absorption and residual stress-focused methods, such as the EN14488-5 square panel test [25] and the EN14488-3 bending beam test [3, 11, 18], respectively.

According to the original DPT configuration proposed and standardized by UNE83515 [28], the perimeter increase must be measured by a circumferential extensometer in the mid-height of the cylinder, which creates difficulties in the test implementation in most laboratories due to its elevated cost. The complexity of the test leads to the search for simplification in standards that may compromise the accuracy of the analysis. An analytical model for converting the vertical displacement measurement into total circumferential opening displacement (TCOD) was proposed [29] to dispense the use of the extensometer and make the test procedure easier. This proposal was validated experimentally with an error lower than 6.7% [30], indicating reduced variability. Extra validation into the analytical conversion model by different measurement methods could provide more trustworthiness to the DPT. Regarding that, innovative methods such as the 3D digital image correlation (DIC3D) have emerged as reliable [31] and, over time, gradually easier to access alternatives for all abroad laboratories. Although this, some standard procedures, such as the Brazilian Standard ABNT NBR16939 [32], allow the use of different dimensions of cylinders using only displacement control and excluding the requirement of controlling the TCOD by a circumferential extensometer.

The DPT still deserves a better understanding of the test mechanism, which depends on a series of fiber-matrix interactions that are more complex than the bending tests [33]. In addition, the test setup itself can alter the test responses influencing the instability extension level and, consequently, the determination of residual strengths in the region of low displacement level [34]. However, this aspect was not evaluated in terms of the dimensions of the specimens.

Although previous studies provide good correlations between the DPT and other methods to control FRS [11, 25], it is essential to consider the crack opening level and not only the level of displacement. It occurs because the crack opening is directly linked to the assessment of the material qualification for structural purposes in terms of residual strength associated with the service limit state (SLS) and ultimate limit state (ULS) [35], which is a new trend regarding FRS applied in tunnel linings [36]. Therefore, the present experimental study provides a better understanding of the DPT mechanism to evaluate its applicability as a quality control method for FRS structural behavior. In that sense, the scope of the study is to verify the influence of the diameter of the specimens on the control of the material by axial displacement monitoring, considering the determination of residual strengths associated with the SLS and ULS.

2. EXPERIMENTAL PROGRAM

To guarantee the adequate replication of the conditions of the shotcrete application as a tunnel lining material, the specimens were produced from extracted cores from test panels produced in a tunnel construction site in São Paulo, Brazil ("Rodoanel - Lote 5" by the Construcap-Copasa consortium) according to the Brazilian Standard ABNT NBR13070 [37]. A wet-mix shotcrete equipment was used during the shooting process.

2.1. Raw materials and mix design

The contractor group (Construcap-Copasa) supplied the raw materials and developed the shotcrete mix design used in the experimental program and tunnel lining production. The mix design of FRS and the geometrical and mechanical properties of the steel fibers are shown in Table 1 and Table 2, respectively. The maximum size of the aggregates was 10 mm, which is typically used in shotcrete to avoid clogging, and it is in accordance with the ACI aggregate grading n. 2 [38]. The steel fiber used in the experiment is typical hooked-end fiber, as illustrated in Figure 1. The specified characteristic compressive strength of the shotcrete was 30 MPa.

2.2. Production of the specimens

The specimens were produced from extracted cores from test panels with the geometry presented in Figure 2. A total of 21 specimens were tested, including 12 specimens with 10 cm diameter and 9 with 15 cm diameter. The cores were extracted from three different test panels (Figure 3). After the extractions, the specimens have identified their top and bottom surfaces to guarantee that all specimens are tested with the same orientation and position at the test machine. The face in contact with the test panel mold was assigned as the "bottom" and the opposite as the "top".

Table 1: Mix design of FRS.

High strength Portland type cement (kg/m^3)	430
Natural sand (kg/m^3)	263
Artificial sand (kg/m^3)	1004
Coarse aggregate (kg/m^3)	434
Water (kg/m^3)	206
Plasticizer (*Glenium*) (l/m^3)	2.58
Accelerator (*MasterRoc**) (l/m^3)	13

*The subspecifications of the GLENIUM® and MasterRoc® additives used in the concrete mix design were not informed.

Table 2: Geometrical and mechanical properties of the steel fibers (data provided by the manufacturer).

TYPE OF FIBER	**DRAMIX® 3D 45/35 BL**
Length L_f	35 mm
Diameter ∅	0.75 mm
Aspect ratio L_f / ∅	45
Tensile strength f_{uf}	1225 MPa
Young's modulus E_{sf}	210 GPa
Poisson's ratio v	0.3

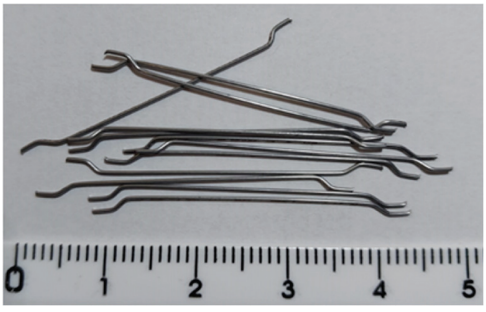

Figure 1: Steel fiber used in the experimental program.

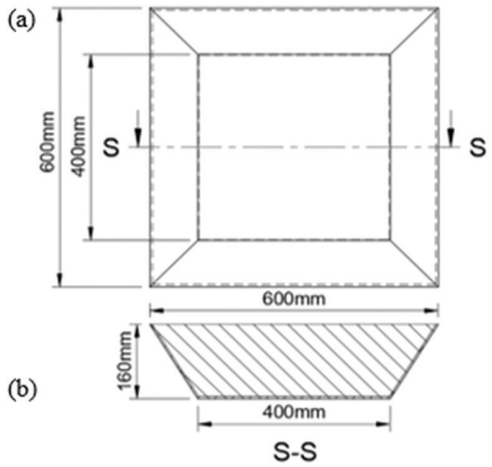

Figure 2: Geometry of the test panels used in the experiment: (a) bottom view; and (b) cross-section.

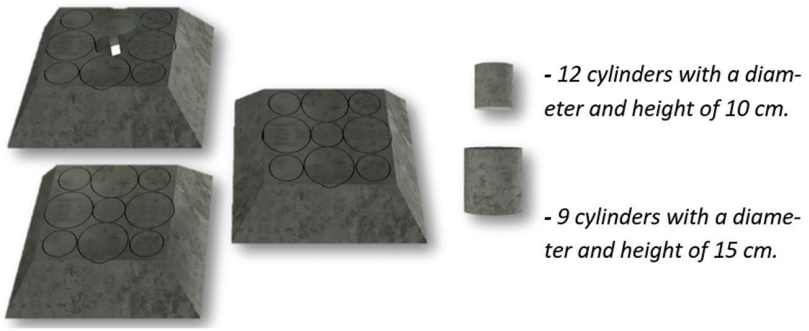

Figure 3: Arrangement used for the extraction of cores from shotcrete panels.

The cores extractions were conducted as illustrated in Figure 4. Subsequently, the extra height in each core was cut off to ensure that the cylindrical specimens had heights of 10 cm and 15 cm, maintaining the 1:1 height:diameter proportion. At last, the top surfaces of the cylinders were also rectified and polished. This procedure guaranteed a good contact surface with the steel loading discs, avoiding any undesired stress concentration in this region [39].

2.3. Test methods

All the tests were performed when the shotcrete was over 50 days old. This procedure mitigates any possible influence of the hydration conditions of the material once accelerators and high early-strength cement are used in the shotcrete. Previously to the DPT, each specimen was evaluated by the inductive test method to determine the steel fiber content. 3 specimens were tracked by DIC3D equipment for each series, totalizing 6 DPT tests monitored by this method. As these tests are not frequently described in standards, a more detailed explanation is provided in the following items.

2.3.1. Inductive test method

The inductive method measures the inductance variation caused by the steel fibers present in each specimen [13–15]. The procedure was previously used to determine the fiber content in shotcrete [3, 11] and allows the use of the same cylindrical specimen for the DPT. The inductive method consists of an LCR impedance analyzer and a circular coil that receives an electric current and generates a magnetic field. In the configuration used in the experiment, the coil is circular, with two windings of 1200 turns each, produced with copper wire 0.3 mm in diameter. As the magnetic field formed is not altered by the plain concrete, the alterations can be associated with the amount of steel fibers present in the specimen. The determinations are made with three positioning orientations of the specimen inside the coil: axial (Z), initial diametrical (0°) and orthogonal

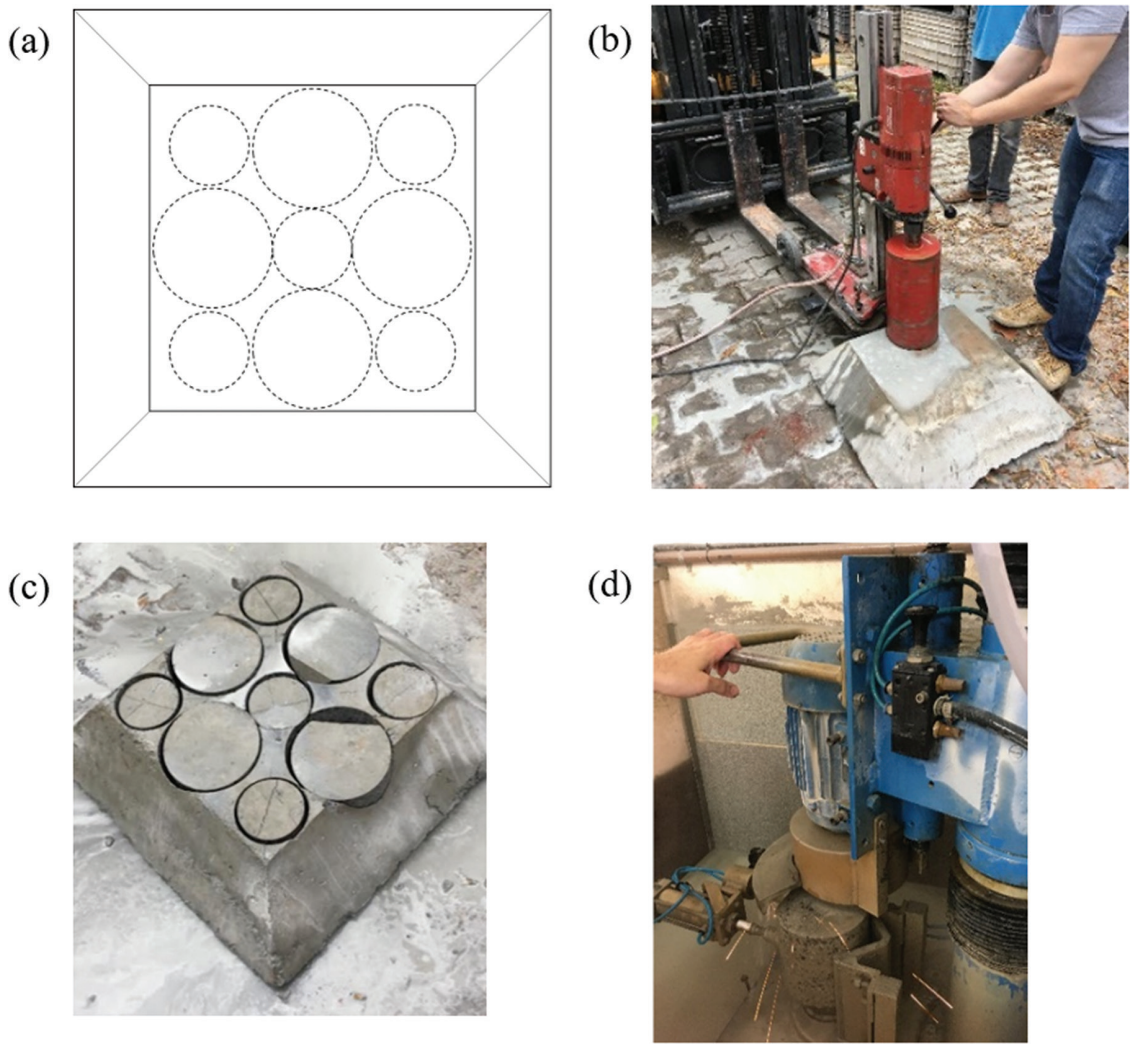

Figure 4: The core extractions: (a) extraction arrangement; (b) cylinders extraction procedure; (c) square panel aspect after the extraction; and (d) surface polishing.

diametrical to anterior (90°). The correlation with the fiber content is then performed using the total inductance corresponding to the sum of the inductances obtained in the three measurement directions.

A calibration should be carried out previously to the test program using the same steel fiber type with similar content. The dosages used for the calibration varied from 15 and 45 kg/m^3 to cover the more typical range used in tunnel lining and the content used in this experimental plan. The fibers were introduced in styrofoam cylinders with the geometry of the real shotcrete specimens. The volumes of the cylinders were 785.40 cm^3 and 2650.72 cm^3 for the diameter of 10 cm and 15 cm, respectively, in which were inserted the amounts of 11.78 and 35.34 g for the ones with 10 cm, representing respectively 15 and 45 kg/m^3, and, as the same proportion, 39.78 and 119.24 g for the ones with 15 cm. The calibration results are shown in Table 3 and Figure 5. The fiber content determination is the same used by CÁCERES *et al.* [11]. For this, the dimensions of height and circumferences of the base and top of the specimens were measured, as well as the inductance levels inferred from the fiber mass.

2.3.2. Digital image correlation analysis

In this study, a partial circumferential displacement of the specimen was measured by a DIC3D system during the DPT. This method was chosen because it provides better measurement accuracy on cylindrical surfaces than other methods applicable to flat surfaces [40, 41]. The methodology was applied during the DPT execution of 3 cylinders of each diameter, and then the measurements were compared against the TCOD obtained analytically by the equations described forward.

Table 3: Inductance calibration.

TEST ORIENTATION MEASUREMENT	SPECIMENS: 10 cm				SPECIMENS: 15 cm			
Axial Z	0.312	mH	0.911	mH	0.903	mH	2.740	mH
Diametrical 0º	0.467	mH	0.989	mH	1.078	mH	3.465	mH
Diametrical 90º	0.307	mH	1.056	mH	1.179	mH	3.651	mH
TOTAL INDUCTANCE	1.083	mH	2.956	mH	3.160	mH	9.857	mH

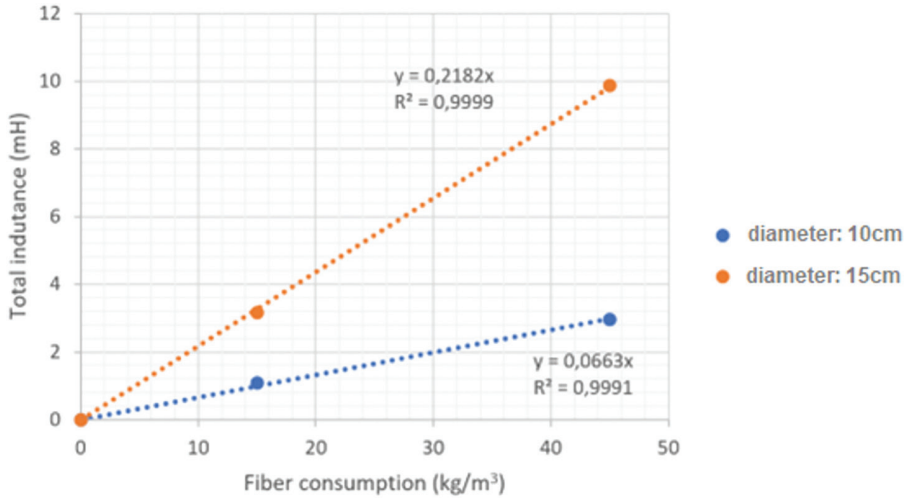

Figure 5: Interpolation calibration results for specimens with 10 cm and 15 cm diameters.

The digital image correlation (DIC) is a non-contact and non-destructive measurement photogrammetry method, proven accurate and widely accepted in civil, mechanical, and aerospace engineering [31, 42, 43]. However, two or more cameras must be used for depth measurements and tridimensional results to allow triangulation algorithms application to determine depth data.

This photogrammetry method allows an alternative to the DPT extensometer chain in this experiment. One of the main advantages is that DIC does not present contact and slipping problems like traditional methods. Also, this method verifies the specimen's circumferential deformation over the entire height and not only in the central line. This condition provides a greater range of evaluation and a substantial amount of data that can eventually be confronted with numerical models that simulate the DPT conditions.

This type of monitoring equipment can be used to observe particularities that occurred during the tests. For example, the singular case of the FRS DPT allows the evaluation of possible discrepancies along with the cylinders' height, like a possible difference between the perimeter increase at the upper and lower sections.

The superficial defects were filled up by plastering for the specimens' preparation to guarantee a smooth surface. Once the defects were corrected, three layers of white paint were applied by spray. The plastering layer was only applied at specific and discontinuous points so that there were no crack propagation contingencies.

After that, one last random black dot layer, also referred to as a "speckle pattern", was applied by an equipment device similar to a rubber stamp on the specimen surface to obtain references for the DIC use. These procedures are illustrated in Figure 6.

The specimens were monitored by two 5.0 megapixels cameras throughout their entire execution (average time of 14 minutes) using image capture at a rate of 1/3 frame per second (fps), and properly referenced in the testing setup. The setup measured about 1/3 of the cylinder perimeter or equivalent to 120°. Figure 7 shows the equipment set used and how it was displayed. The company LYNX provided the equipment, and the images were processed using the VIC-3D software from Correlated Solutions at UFABC (Federal University of ABC, Brazil) Aerospace Engineering Laboratory.

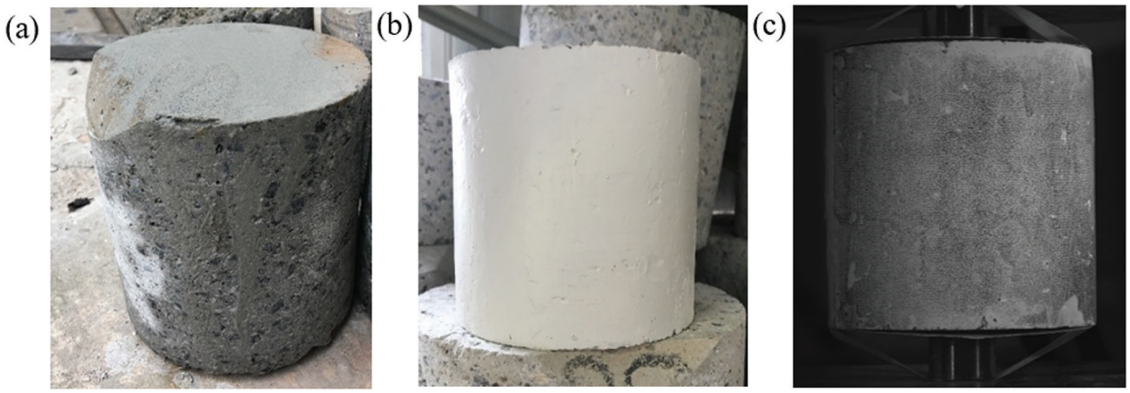

Figure 6: Preparation of the specimens for the DIC: a) specimen extracted from the panel; b) specimen with the plastering fill and white painting layer; and c) specimen with the random black dot pattern layer.

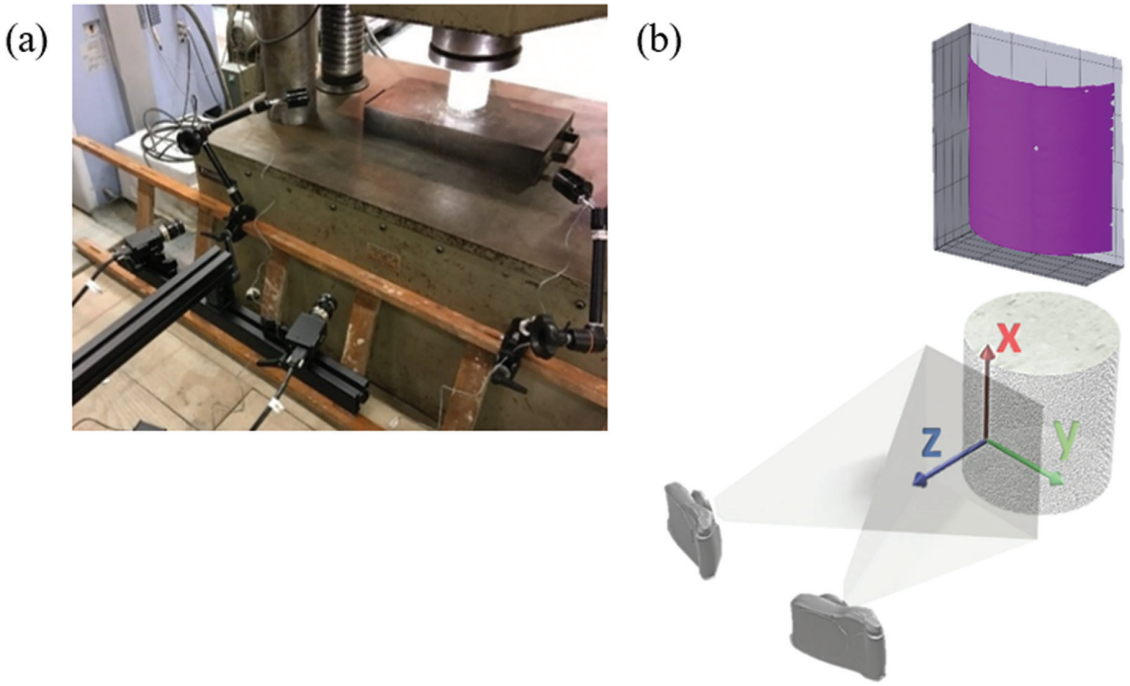

Figure 7: Test arrangement: a) DIC3D equipment setup; and b) representation of the hardware displaying and surface monitoring.

The DIC algorithmic process analyzes a sequence of images to divide the monitored area into regions of subsets of points to track out the deformation (the number of subsets in the monitored area can also be manually defined). The strain field is then calculated from the overlaying of subsets over time, where the positioning of each point is compared with its origin referentially (where the current image is compared with the reference image from the beginning of the trial) or incrementally (comparison of the current image with the previous one). In this study, the correlation of the images is presented by a referential approach since the incremental analysis could result in the accumulation of errors. Figure 8 illustrates the algorithmic process that takes place. Notably, applying the black dot layer (speckle pattern) to be random is important, as it allows the algorithm to differentiate the subsets in the monitored area. Otherwise, the tracking of displacements would be compromised.

Similarly, to control specimens that have three-dimensional surfaces (cylinders, in the case of this study), the use of two cameras allows the triangulation of the points in the subsets and, through computing the cylinder transformation, the possibility of monitoring new variables R, Z (cylinders) and Theta, as well as dR, dZ (cylinders) and dTheta. These refer to the radius (distance from the polar axis), axial coordinate, and rotation angle (in radians), respectively.

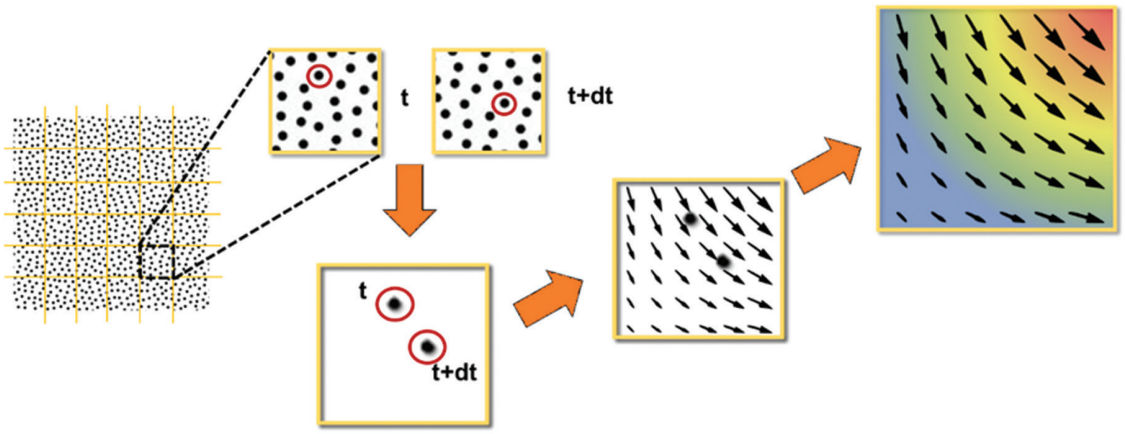

Figure 8: Representation of the subsets and control made by the software (adapted from SUTTON *et al.* [44]).

Despite the scarcity of application of the methodology in civil engineering, the method still stands out for its portability and capacity to obtain true magnitude data, in addition to real-time analysis of strain fields [31].

In this study, the data from DIC3D was used to correlate the load applied and the average diameter increase (dR) of the entire monitored region from the peak load point forward. All results were anchored to the same referential dumping previous variations that may have occurred due to the specimen accommodation in the equipment. Subsequently, the dR data was compared with the TCOD obtained from the analytical conversion of the DPT.

Still exploring the versatility of the DIC3D, the diametrical increments were analyzed separately in the upper and lower portions of the specimens, in addition to the perimeter evaluation simulating a circumference extensometer in the center of the cylinder. Figures 9 and 10 illustrate the data monitored during the tests, with S0 and S1 being the upper and lower portions, respectively, and E0 the virtual strain gauge used.

2.3.3. Double punch test

The DPT tests were carried out according to the standard procedures of ABNT NBR 16939 [32]. The tests were performed in a Shimadzu universal testing machine with a capacity of 200 tf and closed-loop configuration, which is essential for ensuring minor influence in the post-cracking strength determination due to instabilities [34]. According to Brazilian Standard ABNT NBR 16939 [32], the residual strength load values must be controlled by axial displacement referential points of 0.5; 1.5; 2.5 and 3.5 mm from the cracking point (Pf), respectively P0.5, P1.5, P2.5 and P3.5. These displacement values are applied indistinctly to specimens 10 or 15 cm in diameter.

The loading is applied with a constant displacement rate of 0.5 mm/min during the test. The steel discs used to apply the load at the top and bottom part of the specimen have a diameter of 1/4 of the cored cylinder and a height of 1/5 of the specimen. The specimens were always placed with the same orientation, the bottom facing the upper disc and the top facing the lower one. This procedure was followed to mitigate a variable that could interfere with the results. The tensile strength of the FRS is calculated using Equation 1. The parameters used in this calculation are illustrated in Figure 11.

$$f_t = \frac{4P_f}{9\pi aH} \tag{1}$$

where:

f_t = tensile strength (MPa);

P_f = cracking start load (N);

a = diameter of the loaded disc (mm);

H = specimen height (mm).

The fracture pattern that most often occurs in specimens presents three radial cracks, but, in some cases, two or four cracks may occur [45]. These possible crack patterns are illustrated in Figure 12 with some tested

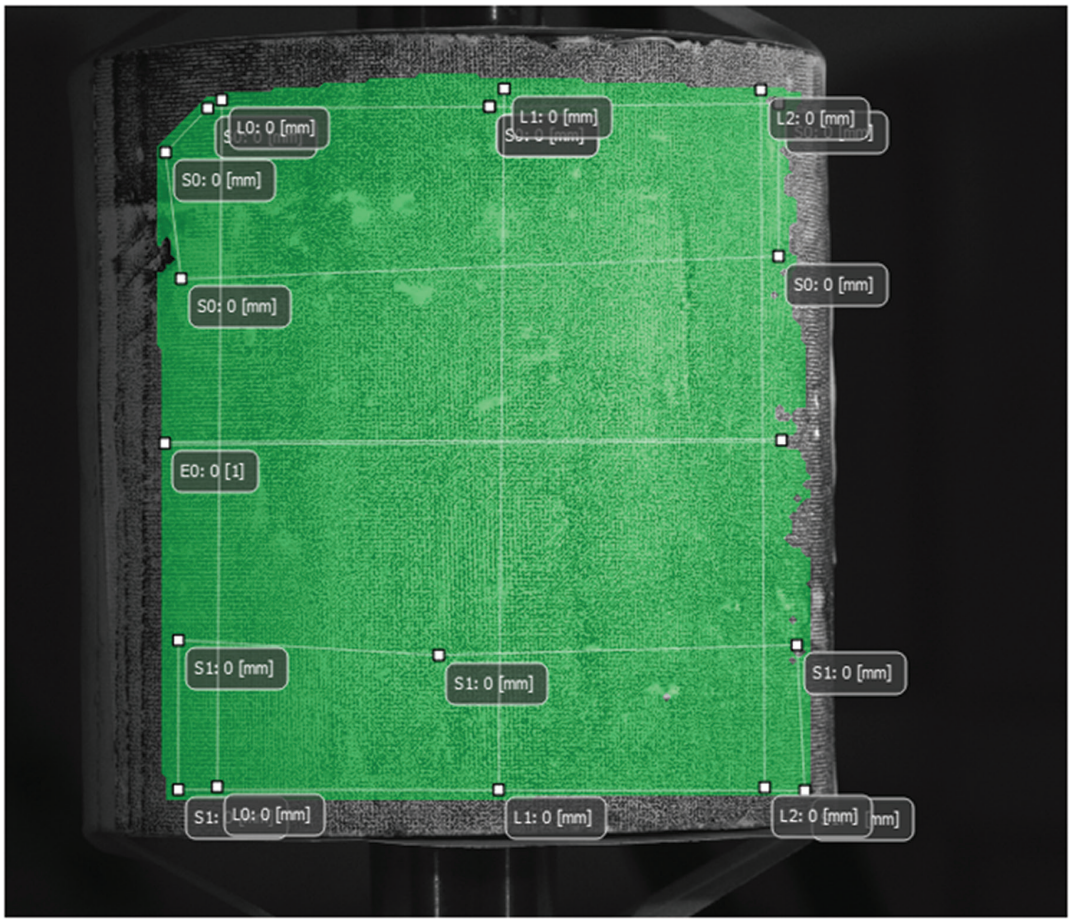

Figure 9: Delimitations monitored on the cylinders: S0, S1 and E0.

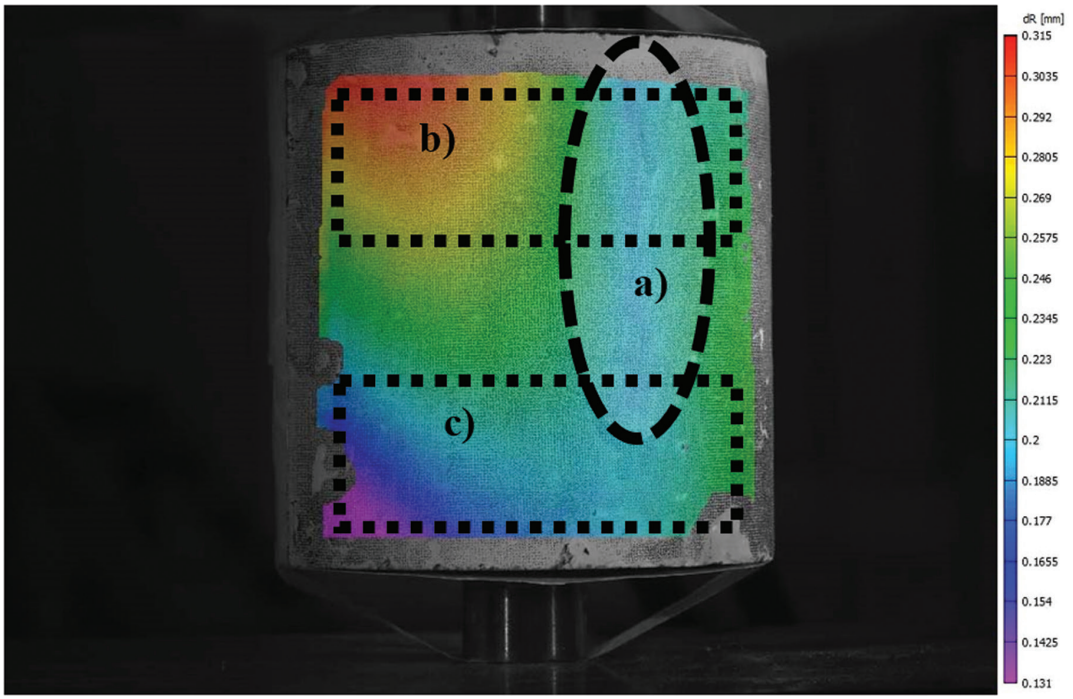

Figure 10: 3D digital image correlation: a) radial crack origin; b) upper section with higher perimeter increase; and c) lower section with lesser perimeter increase.

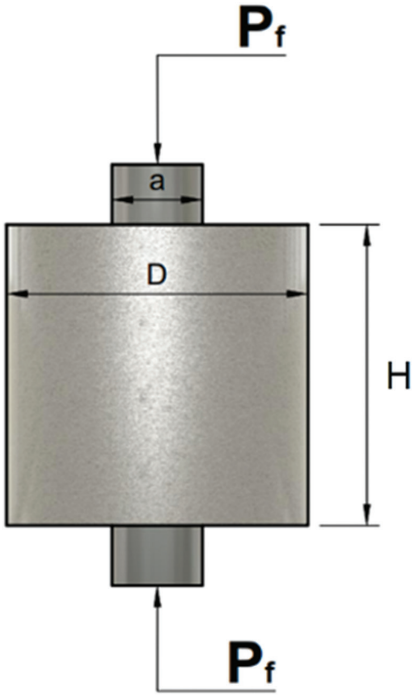

Figure 11: DPT scheme showing the parameters used to determine the peak and residual strength values.

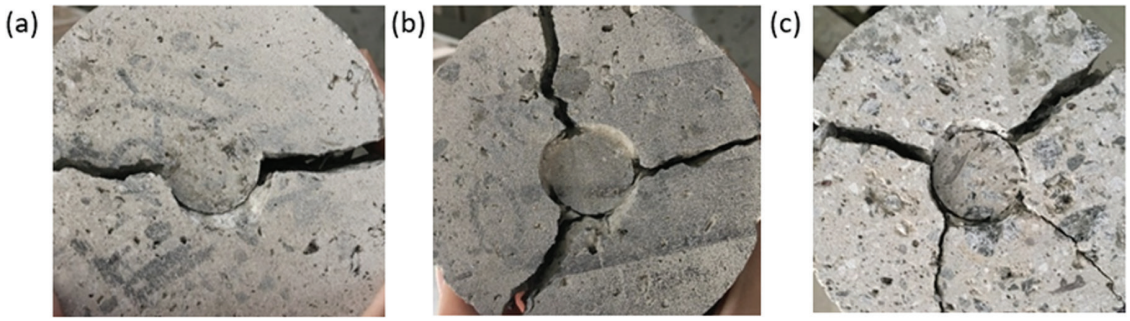

Figure 12: Most common fracture mechanisms occurred in the DPT: (a) two radial fractures; (b) three radial fractures; and (c) four radial fractures.

specimens of the present study. Notably, the number of cracks is input data for the analytical conversion model used to translate axial displacement into TCOD [29].

The wedge lengths of the cones formed during the loading were estimated considering the friction angle of 65° [33, 46]. Figure 13 illustrates the reason employed to establish the correlation between axial displacement and TCOD as described in Equations 2, 3 and 4 according to [29].

$$\text{TCOD} = 0 \text{ if } \delta \leq \delta_{cr} \tag{2}$$

$$\text{TCOD} = n\frac{a\delta_{R,0}}{2l_{wedge}} sin\frac{\pi}{n}\left(1-\frac{F}{F_{cr}}\right) \text{ if } \delta_{cr} < \delta < \delta_{R,0} \tag{3}$$

$$\text{TCOD} = n\frac{a}{2l_{wedge}} sin\frac{\pi}{n}\left[\delta - \delta_{cr} + \delta_{R,0}\left(1-\frac{F_{R,0}}{F_{cr}}\right)\right] \text{if } \delta \geq \delta_{R,0} \tag{4}$$

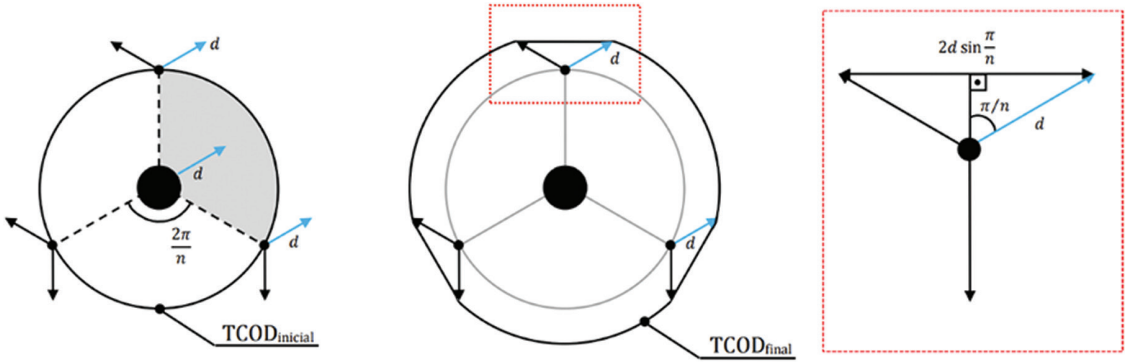

Figure 13: Configuration for the deduction of the axial displacement – TCOD conversion equations (adapted from PUJADAS [29]).

where:

n = number of radial cracks - fracture mechanism;

a = diameter of the loading disc;

l_{wedge} = length of the wedge formed;

F_{cr}, δ_{cr} = force and displacement, respectively, at the point of maximum load;

$F_{R,0}$, $\delta_{R,0}$ = force and displacement, respectively, at the starting point of residual strength.

Equation 1 also helps to determine the residual strength in different levels of circumferential deformation (TCODx) – replacing tensile strength (ft) for residual strength (ftTCODx) and first cracking load (Pf) for the equivalent load to a circumferential deformation (PTCODx).

For the strength *versus* TCOD analysis, a rationale is used to consider reference points and their respective loads associated with SLS and ULS. For the SLS, it was adopted a crack opening of 0.5 mm, which corresponds to a TCOD = 1.5 mm considering the most frequent fracture mechanism of three radial fractures. This adopted value is interesting because it is beyond the reach of the instabilities extents of the DPT. For the ULS, the crack width of 1.5 mm is adopted and corresponds to a TCOD equal to 4.5 mm. Those values are in accordance with the *fib* Model Code 2010 [47] recommendations for failure modes considerations in the ULS.

A sample sizing study was also done considering the residual strength results obtained from the two specimen sizes used in the tests to verify the minimum number of specimens in the sample that provide a representative result. The number of specimens (ns) in each sample was then calculated considering a student's t-distribution given by Equation 5:

$$ns = \frac{Z^2 \cdot SD^2}{(CV \cdot AVG)^2} \tag{5}$$

where:

Z = coefficient obtained directly from the student's t-distribution table;

SD = standard deviation found in each sample;

CV = coefficient of variation in each sample;

AVG = average load of each sample.

3. RESULTS AND DISCUSSION

3.1. Fiber content

The average results of steel fiber contents are presented in Table 4 and demonstrate no significant difference between the series. In addition, the variation of the results was significantly reduced once the coefficient of variation was lower than 8%.

Table 4: Average fiber content and respective standard deviations.

	AVERAGE FIBER CONTENT (kg/m³)	STANDARD DEVIATION (kg/m³)	COEFFICIENT OF VARIATION (%)
10 cm	38.6	3.0	7.8
15 cm	38.3	2.7	7.0
AVERAGE	**38.5**	**2.8**	**7.4**

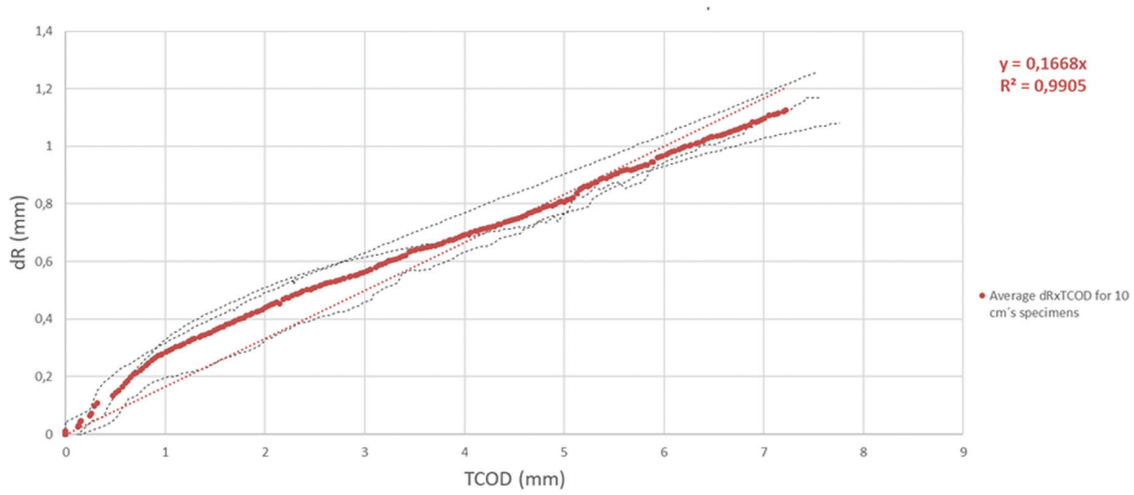

Figure 14: Correlation between the analytical conversion and the DIC3D for the specimens with 10 cm diameter.

3.2. 3D Digital Image Correlation (DIC3D)

The average deformation results (dR) along the complete cylinder height and in its upper (dR S0) and lower (dR S1) deformation portions are presented individually in the appendix with the results obtained from the virtual extensometer E0. Although there are differences in the dR of S0 and S1, these results have no significant differences. The variations occurred randomly without any clear pattern. For the virtual extensometers, the results showed a good correlation between the measurements, indicating that the average monitoring of dR along the height of the cylinder is compatible with the control of the perimeter in the mid-height. The monitoring of the average results in the complete portion is, therefore, more representative of the DPT DIC3D.

Figures 14 and 15 show the correlation between the analytical conversion and the photogrammetry method by specific displacements (dR/diameter and TCOD/perimeter). These correlations were made considering the mean values to minimize the effect of the dispersion of results in determining the geometric relationship between the parameters. In this specific condition, the values of the correlation coefficients were very high and close to one. This demonstrates that the relationship of the parameters is governed by a geometric condition. It is important to mention that during the transition phase of the DPT (the moment right after the cracking loads, where there is an abrupt increase of the diameter), there is less data measured once the pictures are taken in regular intervals. It also reveals that the analytical TCOD corresponds to the results of average values of dR independently of higher variation of this parameter in the regions near the bottom and up facings.

The fact that there is not a perfect relation equal to one between the specific strains measured by the DIC3D and the obtained from the TCOD may be associated with the fact that the DIC3D does not cover the entire perimeter of the specimen. In this sense, there may be a concentration of strain in the DIC3D observation area, for example, which generates an increase in the specific strain. However, the correspondence remains observed, and the average measurement can be considered representative of the existing strains along with the specimen's entire height.

3.3. Double Punch Test

3.3.1. Load *versus* axial displacement

The results of the load applied *versus* the axial displacements are shown in Figures 16 and 17 for the specimens with diameters of 10 cm and 15 cm, respectively. The cracking loads (P_f) are equivalent to the peak load once

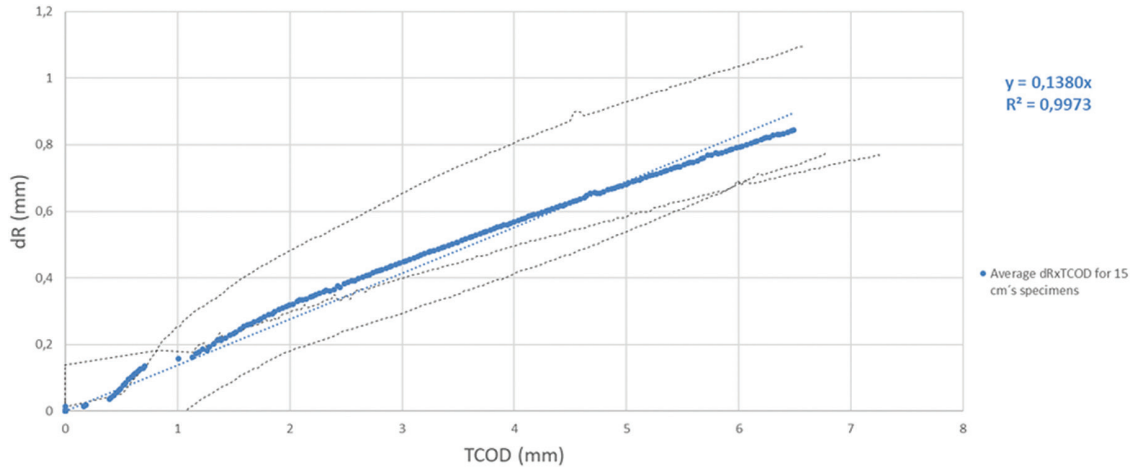

Figure 15: Correlation between the analytical conversion and the DIC3D for the specimens with 15 cm diameter.

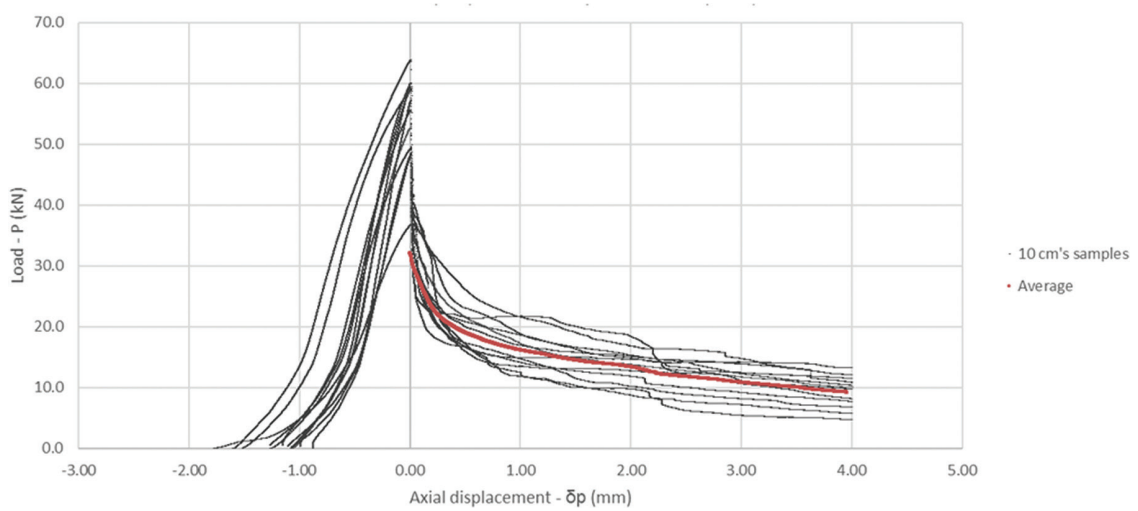

Figure 16: Load applied *versus* axial displacement for the specimens with a diameter of 10 cm.

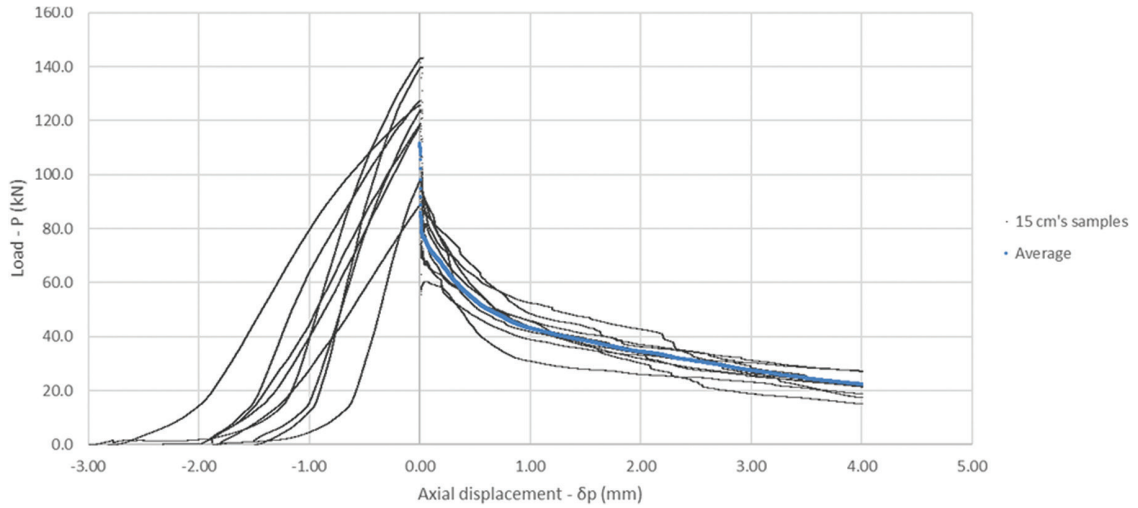

Figure 17: Load applied *versus* axial displacement for the specimens with a diameter of 15 cm.

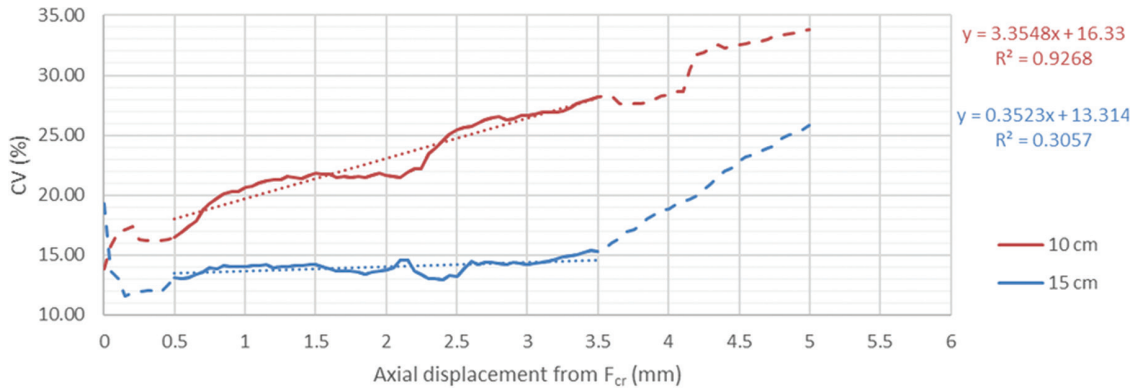

Figure 18: Coefficient of variation on the standard deviation *versus* axial displacement after the critical load.

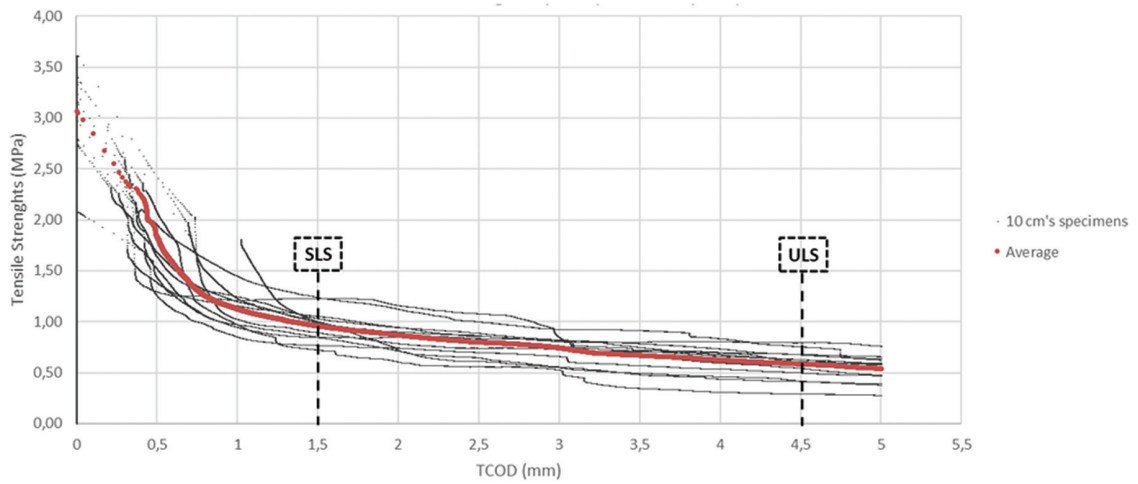

Figure 19: Tensile strength *versus* TCOD for the specimens with a diameter of 10 cm.

there is post-crack softening behavior in all specimens. The abrupt drop indicates the instability associated with the transition phase in the load-bearing capacity of the specimen [34, 39]. It is a typical behavior presented by low fiber content concretes when the difference between the F_{cr} and the residual strength is higher.

The data scatter of the samples is better visualized when considering the coefficient of variation (CV) against axial displacement. The coefficient of variation is the ratio between the standard deviation and the respective sample average value given in percentage. Figure 18 shows the CV values obtained in relation to the axial displacement of the test. The CV values obtained with the specimens with 10 cm are much higher than the ones obtained with specimens with 15 cm. Differences in CV variation trends with axial displacement observed in Figure 18 in relation to different specimen sizes can be attributed to the higher stability level of the test in 15 cm specimens associated with the larger fracture area. In this situation, there is a smaller dispersion of the results for larger displacements where the behavior is governed by the pullout of the fibers in the region of the crack. As the behaviors were all softening, in which the average value is reduced with increasing displacement, this condition conferred the stability observed for the CVs of these specimens up to a displacement of 3.5 mm. More important, the difference between the CVs is greater in the range of controlled interval varying from 0.5 mm to 3.5 mm of axial displacement. As the resisted load values are lower for the smaller specimens and considering that the standard deviations are relatively close, there is greater uncertainty for the 10 cm specimens in terms of determining average values. This condition is intensified with the increase in displacement, which generates a reduction of the average values due to the softening behavior and, consequently, an increase in CV values.

3.3.2. Tensile strength *versus* TCOD

According to the procedures described in section 2.3.3 by Equations 1 to 4, the results in Figures 19 and 20 are presented as residual strength (MPa) *versus* TCOD (mm). The average values for $f_{1.5}$ and $f_{4.5}$ are, respectively, 0.97 MPa and 0.58 MPa with 16.8% and 25.8% of the coefficient of variation for the 10 cm and 1.37 MPa and

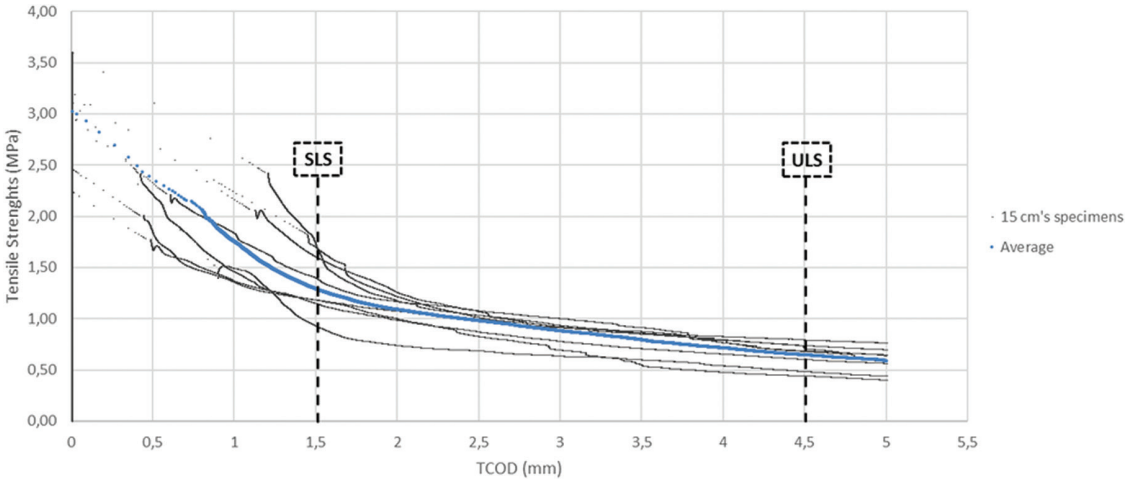

Figure 20: Tensile strength *versus* TCOD for the specimens with a diameter of 15 cm.

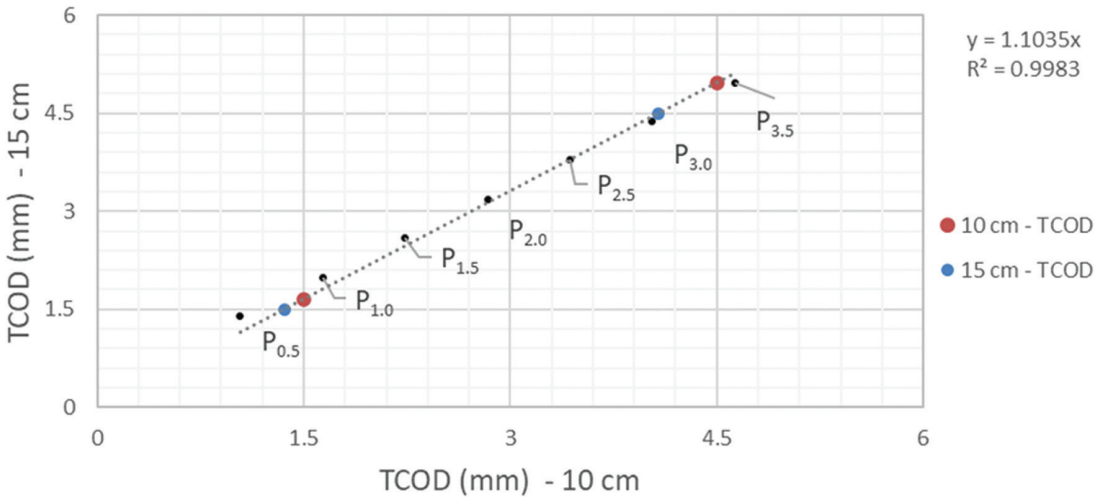

Figure 21: TCOD correlation for the same control points.

0.64 MPa with 18.9% and 16.9% CV for the 15 cm. Figure 21 presents the TCOD measured of each diameter for the presented axial displacements control points, it is then possible to figure out that the reference loads, associated with the vertical displacement, occur in the 15 cm specimens for TCOD levels 10% higher than in the 10 cm specimens. As a result, these forces do not perfectly correspond to the same average crack opening level.

Also, it is possible to verify that both diameters have very similar results for the residual strengths associated with the ULS and the Fcr, with a difference in the average values of 10,5% and 1,3%, respectively. In opposition, residual strengths associated with the SLS presented significant differences from the mean value of approximately 35%, as shown in Figure 22 and Tables 5 and 6. Thus, it is possible to conclude that there is a risk of underestimating the residual strength of the FRS associated with the SLS when using smaller specimens in the DPT test. It is essential to emphasize that the differences found in the steel fiber amount through the inductive method were not significant since both diameters' cores were extracted from the same panels. Thus, the differences in the results obtained for the post-cracking residual strength depend mainly on the DPT dynamics. The execution of a paired t-test for the TCOD control points shows that from the 0.5 to 2.0 stretch, the hypothesis of difference between the samples can be considered true and, in the other measures, this hypothesis can be considered null, as shown in Table 7.

3.3.3. Sizing sample results for TCOD

The sizing of the sampling was performed using the data obtained for residual stresses in the cores for the two diameters of the specimens. For this procedure, it was considered the reliability of 95% and a student's t

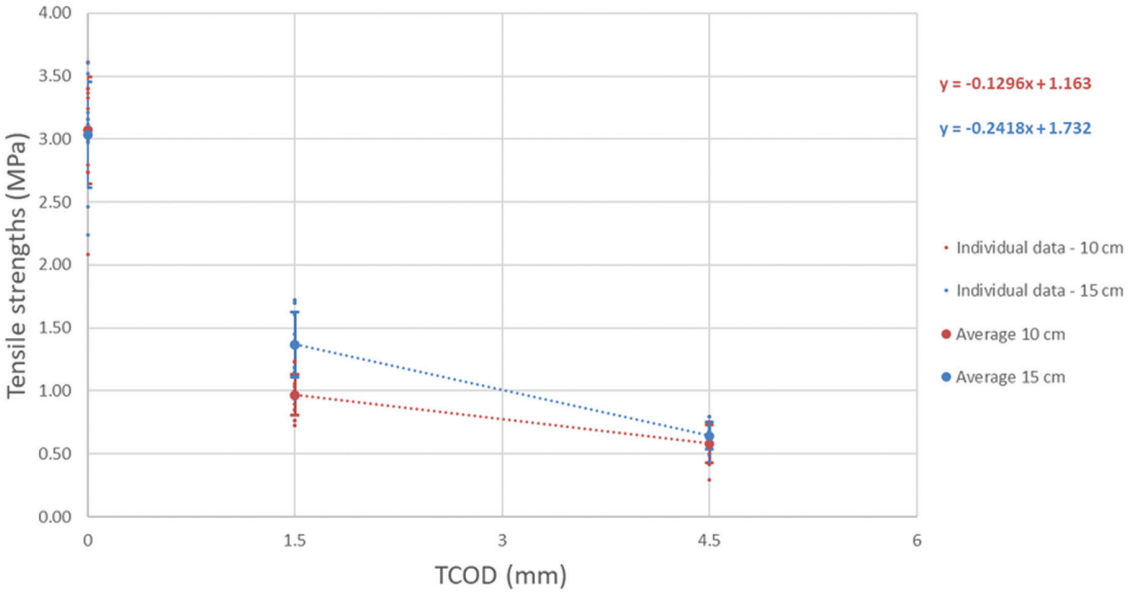

Figure 22: SLS (1.5 mm) and ULS (4.5 mm) points of tensile strength *versus* TCOD.

Table 5: Residual strength (MPa) at TCOD points – 10 cm specimens.

	10_1	10_2	10_3	10_4	10_5	10_6	10_7	10_8	10_9	10_10	10_11	10_12	Average	Std. Dev.	Coef. Var.
F_{cr}	2.98	2.08	3.36	2.79	2.74	3.62	3.33	3.16	2.73	3.24	3.40	3.40	**3.07**	0.42	13.8%
$F_{0.5}$	1.68	1.43	2.45	1.51	1.63	2.47	2.54	1.29	1.25	1.94	2.07	1.38	**1.80**	0.48	26.4%
$F_{1.0}$	1.20	0.95	1.82	0.97	1.25	1.22	1.02	1.21	0.85	1.45	0.97	1.16	**1.17**	0.26	22.5%
$F_{1.5}$	1.00	0.85	1.00	0.85	1.03	0.99	0.89	1.23	0.77	1.24	0.72	1.05	**0.97**	0.16	16.8%
$F_{2.0}$	0.87	0.85	0.72	0.71	0.94	0.90	0.79	1.16	0.74	1.13	0.61	0.95	**0.86**	0.17	19.1%
$F_{2.5}$	0.81	0.84	0.65	0.61	0.89	0.86	0.74	1.08	0.70	1.00	0.56	0.86	**0.80**	0.16	19.4%
$F_{3.0}$	0.76	0.81	0.56	0.55	0.82	0.82	0.73	0.85	0.66	0.93	0.53	0.81	**0.74**	0.13	17.9%
$F_{3.5}$	0.71	0.80	0.48	0.50	0.75	0.79	0.71	0.67	0.57	0.92	0.35	0.72	**0.66**	0.16	24.1%
$F_{4.0}$	0.66	0.81	0.44	0.46	0.68	0.74	0.69	0.60	0.54	0.83	0.31	0.70	**0.62**	0.16	25.3%
$F_{4.5}$	0.63	0.80	0.42	0.42	0.63	0.68	0.61	0.55	0.50	0.76	0.29	0.68	**0.58**	0.15	25.8%

Table 6: Residual strength (MPa) at TCOD points – 15 cm specimens.

	15_1	15_2	15_3	15_4	15_5	15_6	15_7	15_8	15_9	Aver-age	Std. Dev.	Coef. Var.
F_{cr}	2.46	2.99	3.52	3.16	3.61	3.12	3.21	2.24	2.97	**3.03**	0.42	13.8%
$F_{0.5}$	1.83	2.32	2.56	2.92	3.42	2.21	2.85	1.67	2.33	**2.46**	0.52	21.0%
$F_{1.0}$	1.36	1.49	1.78	2.25	2.77	1.46	2.17	1.37	1.83	**1.83**	0.45	24.8%
$F_{1.5}$	1.19	0.93	1.45	1.70	1.72	1.18	1.61	1.15	1.40	**1.37**	0.26	18.9%
$F_{2.0}$	1.08	0.74	1.31	1.22	1.17	1.00	1.26	0.99	1.17	**1.10**	0.16	14.9%
$F_{2.5}$	1.00	0.69	1.19	1.01	1.04	0.83	1.08	0.87	1.07	**0.98**	0.14	14.7%
$F_{3.0}$	0.92	0.64	1.09	0.92	0.94	0.70	1.00	0.78	0.91	**0.88**	0.14	15.6%
$F_{3.5}$	0.85	0.60	0.89	0.86	0.86	0.55	0.92	0.71	0.88	**0.79**	0.13	16.3%
$F_{4.0}$	0.79	0.54	0.76	0.83	0.80	0.48	0.77	0.66	0.79	**0.71**	0.12	16.5%
$F_{4.5}$	0.74	0.49	0.64	0.80	0.71	0.44	0.69	0.61	0.68	**0.64**	0.11	16.9%

Table 7: Paired samples t-test.

PAIRED SAMPLES T-TEST					
			STATISTICS	gl	p
10 cm - F_{cr}	15 cm - F_{cr}	Student-t	–0.260	8.00	0.802
10 cm - $F_{0,5}$	15 cm - $F_{0,5}$	Student-t	–2.881	8.00	0.020
10 cm - $F_{1,0}$	15 cm - $F_{1,0}$	Student-t	–3.471	8.00	0.008
10 cm - $F_{1,5}$	15 cm - $F_{1,5}$	Student-t	–3.774	8.00	0.005
10 cm - $F_{2,0}$	15 cm - $F_{2,0}$	Student-t	–2.764	8.00	0.025
10 cm - $F_{2,5}$	15 cm - $F_{2,5}$	Student-t	–2.042	8.00	0.075
10 cm - $F_{3,0}$	15 cm - $F_{3,0}$	Student-t	–1.901	8.00	0.094
10 cm - $F_{3,5}$	15 cm - $F_{3,5}$	Student-t	–1.650	8.00	0.138
10 cm - $F_{4,0}$	15 cm - $F_{4,0}$	Student-t	–1.174	8.00	0.274
10 cm - $F_{4,5}$	15 cm - $F_{4,5}$	Student-t	–0.865	8.00	0.412

Note: $H_a\ \mu_{Measure\ 1 - Measure\ 2} \neq 0$

Table 8: Sizing results considering the discussed inputs.

	SPECIMENS – 10 cm RELIABILITY 95%			SPECIMENS – 15 cm RELIABILITY 95%		
TENSILE STRENGTH AT THE TCOD POINTS	AVERAGE (MPa)	Std Dev (MPa)	SIZING (ns)	AVERAGE (MPa)	Std Dev (MPa)	SIZING (ns)
F_{cr}	3.07	0.42	2	3.03	0.44	3
SLS - $F_{1.5}$	0.97	0.16	3	1.37	0.27	5
$F_{2.5}$	0.80	0.16	5	0.98	0.15	3
$F_{3.5}$	0.66	0.16	7	0.79	0.14	4
ULS - $F_{4.5}$	0.58	0.15	8	0.64	0.12	4

distribution (10 cm: Z = 2.201, 15 cm: Z = 2.306) and the sizing was obtained by Equation 5. The coefficient of variation used for the sizing equations was 20%, which corresponds to approximately the average value found on the tests during the residual phase of this study.

The sample results' sizing shows differences in the demanded number of specimens (ns), as presented in Table 8. In general, the specimens with a diameter of 15 cm require a reduced number of specimens in the representative sample mainly because of the lower CV. Therefore, the 10 cm specimen proved advantageous only for determining F_{cr} and $F_{1.5}$, requiring fewer specimens. However, for the post-cracking behavior, the 15 cm specimens proved more effective, requiring a smaller sampling for a higher level of CMOD.

4. CONCLUSIONS

This study focused on evaluating FRS used for structural applications through the double punching test to verify its suitability for quality control. In addition, the study used the simplified displacement control methodology and its verification through DIC3D. This verification proved that the displacement control method is applicable once the analytical equations for converting displacement into TCOD are reliable.

The higher level of control of displacements and deformations used in this experimental study contributed to verifying the great influence of the specimens' dimensions in the double punching test results. Smaller specimens have a smaller fracture area, making the result more dispersed and underestimating the residual strengths compared to those obtained with larger specimens.

Despite the specimens with a 10 cm dimension having been used in important previous works and being permitted by the Spanish and Brazilian standards aiming the test method, it was verified that this dimension underestimates the post-peak residual strengths results at low levels of TCOD associated with SLS in more than 30%. This drawback may be associated with a higher level of post-peak instability, as already evaluated in previous studies once no differences were observed in the actual fiber content.

In addition, a higher number of specimens should be used to assess the results (especially those associated with the ULS) when 10 cm specimens are used. This finding indicates that quality control programs could be hampered by the need to extract a greater number of cores to obtain several specimens suitable for each evaluation. Accordingly, to the exposed, it is evident that using specimens of 15 cm in diameter and height is more effective and reliable for evaluating fiber reinforced shotcrete.

Finally, it is important to mention that the highest confidence level for establishing parameters for regular quality control programs will only be obtained by monitoring real tunnel projects.

5. ACKNOWLEDGMENTS

The authors acknowledge Lynx Comercio e Importação Ltda for providing Correlated Solutions VIC-3D system. The authors also like to extend their acknowledgments to the financial support of the Brazilian National Council for Scientific and Technological Development - CNPq [Grant #142219/2017-7 (Alan Renato Estrada Cáceres); #305055/2019-4 (Antonio Domingues de Figueiredo); #307175/2022-7 and #406205/2021-3 (Luís A. G. Bitencourt Jr.)].

6. BIBLIOGRAPHY

[1] BERNARD, E.S., THOMAS, A.H., "Fibre reinforced sprayed concrete for ground support", *Tunnelling and Underground Space Technology*, v. 99, pp. 103302, 2020. doi: http://dx.doi.org/10.1016/j.tust.2020.103302

[2] FIGUEIREDO, A.D., "Rheological behavior of dry-mix shotcrete", *American Concrete Institute Special Publication*, v.1 86, pp .113–128, 1999.

[3] GALOBARDES, I., SILVA, C.L., FIGUEIREDO, A., *et al*., "Alternative quality control of steel fiber reinforced sprayed concrete (SFRSC)", *Construction & Building Materials*, v. 233, pp. 1008–1015, 2019. doi: http://dx.doi.org/10.1016/j.conbuildmat.2019.08.003

[4] GINOUSE, N., JOLIN, M., BISSONNETTE, B., "Effect of equipment on spray velocity distribution in shotcrete applications", *Construction & Building Materials*, v. 70, pp. 362–369, 2014. doi: http://dx.doi.org/10.1016/j.conbuildmat.2014.07.116

[5] ARMELIN, H.S., "*Rebound and toughening mechanisms in steel fiber reinforced dry-mix shotcrete*", D.Sc. Thesis, University of British Columbia, Vancouver, 1997.

[6] KAUFMANN, J., FRECH, K., SCHUETZ, P., *et al*., "Rebound and orientation of fibers in wet sprayed concrete applications", *Construction & Building Materials*, v. 49, pp. 15–22, 2013. doi: http://dx.doi.org/10.1016/j.conbuildmat.2013.07.051

[7] MORGAN, D.R., CHEN, L., BEAUPRÉ, D., "Toughness of fibre reinforced shotcrete", *Shotcrete for Underground Support*, v. VII, pp. 66–87, 1995.

[8] JOLIN, M., BEAUPRÉ, B., MINDESS, S., "Tests to characterize properties of fresh dry-mix shotcrete", *Cement and Concrete Research*, v. 29, n. 5, pp. 753–760, 1999. doi: http://dx.doi.org/10.1016/S0008-8846(99)00071-X

[9] EUROPEAN STANDARDS, *EN 14488-5: Testing sprayed concrete - Part 5: Determination of energy absorption capacity of fibre reinforced slab specimens*, Germany, European Standards, 2006.

[10] EUROPEAN STANDARDS, *EN 14488-3: Testing sprayed concrete - Part 3: Flexural strengths (first peak, ultimate and residual) of fibre reinforced beam specimens*, Germany, European Standards, 2004.

[11] CÁCERES, A.R.E., MONTE, R., CAVALARO, S.H.P., *et al*., "Alternative small-scale tests to characterize the structural behaviour of fibre-reinforced sprayed concrete", *Construction & Building Materials*, v. 296, pp. 123–168, 2021. doi: http://dx.doi.org/10.1016/j.conbuildmat.2021.123168

[12] EUROPEAN STANDARDS, *EN 14488-7: Testing sprayed concrete - Part 7: Fibre content of fibre reinforced concrete*, Germany, European Standards, 2006.

[13] TORRENTS, J.M., BLANCO, A., PUJADAS, P., *et al*., "Inductive method for assessing the amount and orientation of steel fibers in concrete", *Materials and Structures*, v. 45, n. 10, pp. 1577–1592, 2012. doi: http://dx.doi.org/10.1617/s11527-012-9858-6

[14] LÓPEZ, R., "*Determinación de cuantía y orientación de fibras en HRFA por inducción manética: mejora de un método existente e implantación para probetas cilíndricas*", Universidad Polytécnica de Catalunya, Barcelona. 2013. (In Spanish).

[15] CAVALARO, S.H.P., LÓPEZ, R., TORRENTS, J.M., *et al*., "Improved assessment of fibre content and orientation with inductive method in SFRC", *Materials and Structures*, v. 48, n. 6, pp. 1859–1873, 2015. doi: http://dx.doi.org/10.1617/s11527-014-0279-6

[16] ALFERES FILHO, R.S., MONTE, R., FIGUEIREDO, A.D., "Evaluation of steel fiber orientation in slab elements induced during casting with self-compacting concrete", *Matéria (Rio de Janeiro)*, v. 24, n. 2, pp. e-12340, 2019. doi: http://dx.doi.org/10.1590/s1517-707620190002.0655

[17] BITENCOURT JUNIOR, L.A.G., MANZOLI, O.L., BITTENCOURT, T.N., *et al*., "Numerical modeling of steel fiber reinforced concrete with a discrete and explicit representation of steel fibers", *International Journal of Solids and Structures*, v. 159, pp. 171–190, 2019. doi: http://dx.doi.org/10.1016/j.ijsolstr.2018.09.028

[18] TRINDADE, Y.T., BITENCOURT JUNIOR, L.A.G., MONTE, R., *et al*., "Design of SFRC members aided by a multiscale model: Part I - predicting the post-cracking parameters", *Composite Structures*, v. 241, pp. 112078, 2020. doi: http://dx.doi.org/10.1016/j.compstruct.2020.112078

[19] TRINDADE, Y.T., BITENCOURT JUNIOR, L.A.G., MANZOLI, O.L., "Design of SFRC members aided by a multiscale model: Part II - predicting the behavior of RC-SFRC beams", *Composite Structures*, v. 241, pp. 112079, 2020. doi: http://dx.doi.org/10.1016/j.compstruct.2020.112079

[20] MONTE, R., PEREIRA, L.S., FIGUEIREDO, A.D., *et al*., "Simplified DEWS test for steel fibre-reinforced concrete characterization", *Revista IBRACON de Estruturas e Materiais*, v. 16, n. 6, pp. e16604, 2023. doi: http://dx.doi.org/10.1590/s1983-41952023000600004

[21] PROVIDAKIS, C., TSISTRAKIS, S., VOUTETAKI, M., *et al*., "A new damage identification approach based on impedance-type measurements and 2D error statistics", *Structural Monitoring and Maintenance*, v. 2, n. 4, pp. 319–338, 2015. doi: http://dx.doi.org/10.12989/smm.2015.2.4.319

[22] AGGELIS, D.G., MPALASKAS, A.C., MATIKAS, T.E. "Acoustic monitoring for the evaluation of concrete structures and materials". In: Ohtsu, M. (eds.), *Acoustic emission and related non-destructive evaluation techniques in the fracture mechanics of concrete* (2nd ed), Oxford, Woodhead Publishing, 2021. doi: https://doi.org/10.1016/B978-1-78242-327-0.00013-1

[23] MPALASKAS, A.C., MATIKAS, T.E., AGGELIS, D.G., *et al*., "Acoustic emission for evaluating the reinforcement effectiveness in steel fiber reinforced concrete", *Applied Sciences (Basel, Switzerland)*, v. 11, n. 9, pp. 3850, 2021. doi: http://dx.doi.org/10.3390/app11093850

[24] VOUTETAKI, M.E., NAOUM, M.C., PAPADOPOULOS, N.A., *et al*., "Cracking diagnosis in fiber-reinforced concrete with synthetic fibers using piezoelectric transducers", *Fibers (Basel, Switzerland)*, v. 10, n. 1, pp. 5, 2022. doi: http://dx.doi.org/10.3390/fib10010005

[25] ESTRADA CÁCERES, A.R., CAVALARO, S.H.P., FIGUEIREDO, A.D., "Evaluation of steel fiber-reinforced sprayed concrete by energy absorption tests", *Journal of Materials in Civil Engineering*, v. 33, n. 9, pp. 04021252, 2021. doi: http://dx.doi.org/10.1061/(ASCE)MT.1943-5533.0003865

[26] ESTRADA CÁCERES, A.R., CAVALARO, S.H.P., FIGUEIREDO, A.D., "Integrated approach for quality control of fibre-reinforced sprayed concrete for tunnel lining", *Tunnelling and Underground Space Technology*, v. 140, pp. 105260, 2023. doi: http://dx.doi.org/10.1016/j.tust.2023.105260

[27] MONTEIRO, V.M.A., SILVA, F.A., "The use of the Barcelona test as quality control of fiber reinforced shotcrete for underground mining", *Construction & Building Materials*, v. 262, pp. 120719, 2020. doi: http://dx.doi.org/10.1016/j.conbuildmat.2020.120719

[28] AENOR, *UNE83515: Fibre reinforced concrete. Determination of cracking strength, ductility and residual tensile strength*, Madrid, AENOR, 2010.

[29] PUJADAS, P., "*Caracterización y diseño del hormigón reforzado con fibras plásticas*", D.Sc. Thesis, Barcelona, Universitat Politècnica de Catalunya, 2013.

[30] MONTE, R., TOALDO, G.S., FIGUEIREDO, A.D., "Avaliação da tenacidade de concretos reforçados com fibras através de ensaios com sistema aberto", *Matéria (Rio de Janeiro)*, v. 19, n. 2, pp. 132–149, 2014. doi: http://dx.doi.org/10.1590/S1517-70762014000200008. [In Portuguese].

[31] AMYOT, C.O., PICKWORTH, J., TYSON, J., *et al*. "3D digital image correlation: the ultimate tool for displacements and strains Testing". In: *International Conference on Materials Science & Engineering*, pp. 11, 2019.

[32] ASSOCIAÇÃO BRASILEIRA DE NORMAS TÉCNICAS, *ABNT NBR 16939: Concreto reforçado com fibras - Determinação das resistências a fissuração e residuais a tração por duplo puncionamento – Método de ensaio*, Rio de Janeiro, ABNT, 2021 (In Portuguese).

[33] BLANCO, A., PUJADAS, P., DE LA FUENTE, A., *et al*., "Constitutive model for fiber reinforced concrete based on the Barcelona test", *Cement and Concrete Composites*, v. 53, pp. 327–340, 2014. doi: http://dx.doi.org/10.1016/j.cemconcomp.2014.07.017

[34] SIMÃO, L.C.R., NOGUEIRA, A.B., MONTE, R., *et al*., "Influence of the instability of the double punch test on the post-crack response of fiber-reinforced concrete", *Construction & Building Materials*, v. 217, pp. 185–192, 2019. doi: http://dx.doi.org/10.1016/j.conbuildmat.2019.05.062

[35] THE INTERNATIONAL TUNNELING AND UNDERGROUND SPACE ASSOCIATION, Permanent sprayed concrete linings, *ITAtech Report*, v. 24, pp. 55p, 2020. ITA Working Group no 12.

[36] LARIVE, C., BOUTEILLE, S., BERTHOZ, N., *et al*., "Fiber-reinforced sprayed concrete as a permanent tunnel lining", *Structural Engineering International*, v. 30, n. 4, pp. 1–8, 2020. doi: http://dx.doi.org/10.1080/10168664.2020.1735981

[37] ASSOCIAÇÃO BRASILEIRA DE NORMAS TÉCNICAS, *ABNT NBR 13070: Moldagem de placas para ensaio de argamassa e concreto projetados*, Rio de Janeiro, ABNT, 2012. (In Portuguese).

[38] AMERICAN CONCRETE INSTITUTE, *ACI 506R-16: Guide to Shotcrete. ACI Committee 506*. Detroit, ACI, 2016.

[39] NOGUEIRA, A.B., SIMÃO, L.C.R., MONTE, R., *et al*., "Evaluation of the repeatability and reproducibility of the double punch test", *Construction & Building Materials*, v. 268, pp. 121–145, 2021. doi: http://dx.doi.org/10.1016/j.conbuildmat.2020.121145

[40] DADMAND, B., SADAGHIAN, H., KHALILZADEHTABRIZI, S., *et al*., "Studying the compressive, tensile and flexural properties of binary and ternary fiber-reinforced UHPC using experimental, numerical and multi-target digital image correlation methods", *Case Studies in Construction Materials*, v. 18, pp. e01865, 2023. doi: http://dx.doi.org/10.1016/j.cscm.2023.e01865

[41] DADMAND, B., SADAGHIAN, H., KHALILZADEHTABRIZI, S., *et al*., "Exploring the mechanical properties of steel- and polypropylene-reinforced ultrahigh-performance concrete through numerical analyses and experimental multi-target digital image correlation", *Frontiers of Structural and Civil Engineering*, 2023. In press.

[42] SILVEIRA, M.V.G., BITENCOURT JUNIOR, L.A.G., DAS, S. "A performance-based optimization framework applied to a classical STM-designed deep beam", *Structures*, v. 41, pp. 488–500, 2022.

[43] SILVEIRA, M.V.G., BITENCOURT, L.A.G., DAS, S., "Design and experimental investigation of deep beams based on the Generative Tie Method", *Engineering Structures*, v. 255, pp. 113913, 2022. doi: http://dx.doi.org/10.1016/j.engstruct.2022.113913

[44] SUTTON, M.A., ORTEU, J.J., SCHREIER, H., *Image correlation for shape, motion and deformation measurements*, New York, Springer, 2009. doi: https://doi.org/10.1007/978-0-387-78747-3_1

[45] MOLINS, C., AGUADO, A., SALUDES, S., " Double Punch Test to control the energy dissipation in tension of FRC (Barcelona Test)", *Materials and Structures*, v. 42, n. 4, pp. 415–425, 2008. doi: http://dx.doi.org/10.1617/s11527-008-9391-9

[46] MONTE, R., DE LA FUENTE, A., FIGUEIREDO, A.D., *et al*., "Barcelona test as an alternative method to control and design fiber-reinforced concrete pipes", *Structural Journal*, v. 113, n. 6, pp. 1175–1184, 2016. doi: http://dx.doi.org/10.14359/51689018

[47] FÉDÉRATION INTERNATIONALE DU BÉTON, *FIB model code for concrete structures 2010*, Switzerland, FIB, 2013.

SUPPLEMENTARY MATERIAL

The following online material is available for this article:

Figure S1 - Axial force (kN) *versus* dR (mm) for specimen 10 with 10 cm diameter.

Figure S2 - Axial force (kN) *versus* dR (mm) for specimen 11 with 10 cm diameter.

Figure S3 - Axial force (kN) *versus* dR (mm) for specimen 12 with 10 cm diameter.

Figure S4 - Axial force (kN) *versus* dR (mm) for specimen 7 with 15 cm diameter.

Figure S5 - Axial force (kN) *versus* dR (mm) for specimen 8 with 15 cm diameter.

Figure S6 - Axial force (kN) *versus* dR (mm) for specimen 9 with 15 cm diameter.

Figure S7 - Comparison between the perimeter measured by the virtual extensometer E0 and the diameter increase results of dR for specimens with 10 cm diameter.

Figure S8 - Comparison between the perimeter measured by the virtual extensometer E0 and the diameter increase results of dR for the specimens with 15 cm diameter.